Optics Communications ▮ (▮▮▮▮) ▮▮▮–▮▮▮

Contents lists available at ScienceDirect

Optics Communications

journal homepage: www.elsevier.com/locate/optcom

Harmonic generation microscopy of bone microenvironment *in vivo*

Pei-Chun Wu [a,b], Yu-Fang Shen [c], Chi-Kuang Sun [d,e], Charles P. Lin [f], Tzu-Ming Liu [a,b,*]

[a] Faculty of Health Sciences, University of Macau, Macao
[b] Molecular Imaging Center, National Taiwan University, Taipei 10617, Taiwan
[c] Department of Bioinformatics and Medical Engineering, Asia University, Taichung 41354, Taiwan
[d] Graduate Institute of Photonics and Optoelectronics, National Taiwan University, Taipei 10617, Taiwan
[e] Department of Electrical Engineering, National Taiwan University, Taipei 10617, Taiwan
[f] Wellman Center for Photomedicine and Center for Systems Biology, Massachusetts General Hospital, Boston, MA 02114, USA

ARTICLE INFO

Keywords:
Osteocyte
Bone marrow
Cr:forsterite
Femtosecond
Third harmonic generation

ABSTRACT

Here we report and review the investigation of bone microenvironment *in vivo* with harmonic generation microscopy. Excited by an infrared femtosecond laser, the second harmonic generation images can reveal the bone structures and boundaries. The third harmonic generation images can reveal the osteocytes, connecting canaliculi, and granular bone marrow cells. These imaging features can be used to observe and analyze the histology of the bone microenvironment in the future.

1. Introduction

Label-free second harmonic generation (SHG) and third harmonic generation (THG) contrasts have been widely used for the sectioning imaging of biomedical tissues both *ex vivo* and *in vivo*. The imaging signals depend nonlinearly on the excitation intensity of femtosecond lasers and can only be efficiently generated around the focal point. The out-of-focus background interference can thus be greatly reduced. Compared with the reflectance confocal microscopy excited at the same wavelength, the spatial resolution can also be improved by a factor of $\sqrt{2}$ and $\sqrt{3}$ for SHG and THG microscopy, respectively [1]. By scanning the laser beam, the sectioning images can be point-by-point obtained without a confocal pinhole. Compared with two-photon [2] or three-photon fluorescence [3] microscopy, the SHG and THG contrasts has less molecular but more morphological information. Since they are virtual state transitions, the signals can be excited at a near-infrared wavelength, which falls within the penetration window of most biological tissues and does not photobleach. The SHG contrast needs a non-central symmetry of materials and can effectively reveal the extracellular collagen networks [4–12]. Bone, as mineralized collagens, also have strong SHG signals [11]. On the other hand, SHG signals are usually undetectable within cells unless there are structured proteins like spindle fibers [13]. This modality can be used to identify collagen remodeling in tumor microenvironment [6], fibrosis in liver tissues [7], structural alteration in corneal edema [8], calcified plaques in atherosclerosis [9], the diagnosis of atrial fibrillation [10], the deformation of cartilage microstructures in osteoarthritis [11], and the boundaries of bone marrow cavities [12]. The THG contrast, different from SHG, can be generated even in homogeneous media. But due to a Gouy phase shift, the third-harmonic electric field generated before and after the focus will cancel each other. Therefore, only tight focusing at the interface of materials with different refractive indices or $\chi^{(3)}$ can generate detectable THG signals. With excitation at around 1200–1300 nm, the THG microscopy can reveal cellular morphology, subcellular organelles, and melanin distributions in deep tissues for the application of developmental biology [13,14] and clinical diagnosis [15–17] without labeling. In deep tissues, this technique has less background interference than reflectance confocal microscopy and better transverse resolution (~500 nm) [17] than infrared-laser based μ-optical coherence tomography (OCT) [18] and spectrally encoded confocal microscopy [19]. Recently, our group demonstrated that 30 Hz frame-rate THG microscopy at 1200–1300 nm excitation wavelength can *in vivo* capture the images of human blood cells and resolve their dynamic morphologies [20]. Simply using the cross-sectional area and the average THG intensity in the 2D THG microscopy, three major types of human leukocytes (neutrophils, monocytes, and lymphocytes) can be differentiated with high sensitivity and specificity [21]. This is because THG microscopy is a modality sensitive to intracellular lipids, which is a characteristic feature of leukocytes [21]. These results indicated that harmonic generation microscopy is a powerful method for label-free imaging of tissue both *ex vivo* and *in vivo*, such that

* Corresponding author at: Faculty of Health Sciences, University of Macau, Macao.
E-mail address: tmliu@umac.mo (T.-M. Liu).

https://doi.org/10.1016/j.optcom.2018.01.023
Received 1 September 2017; Received in revised form 23 November 2017; Accepted 13 January 2018
Available online xxxx
0030-4018/

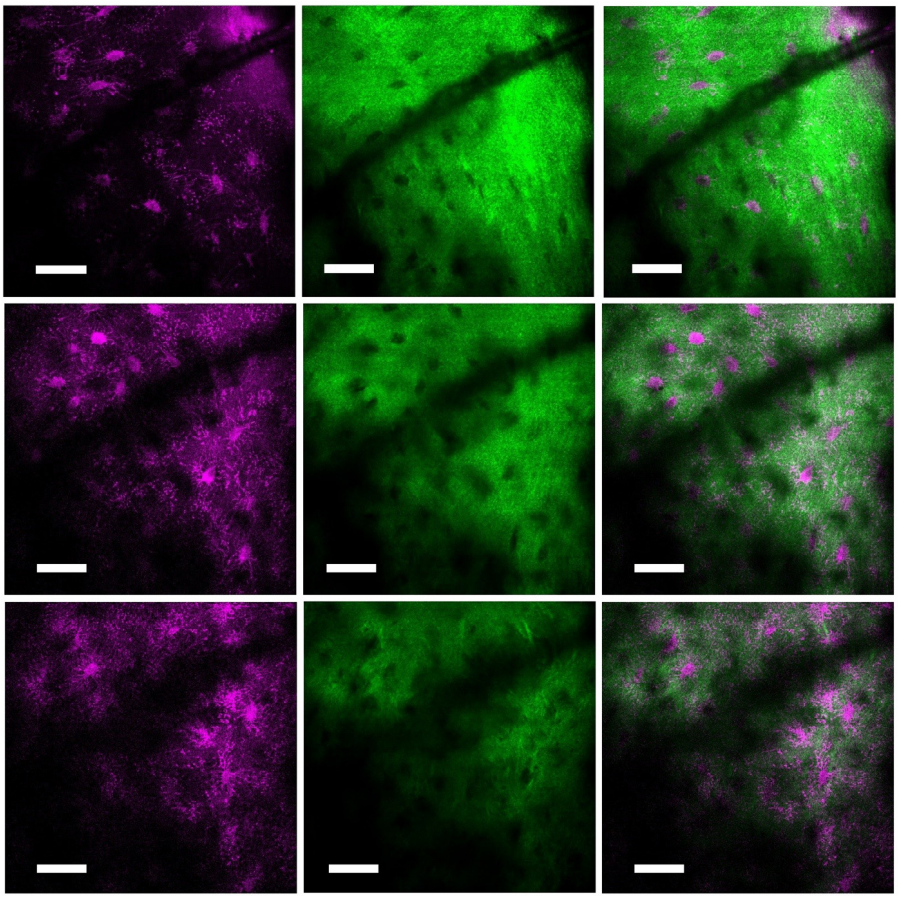

Fig. 1. Third harmonic generation (left column), second harmonic generation (middle column), and combined (right column) images of the calvarial bone of a mouse at the imaging depth of 20 μm (first row), 40 μm (second row), and 60 μm (the bottom row). Fields of view: 240 × 240 μm. Scale bars: 40 μm. (For interpretation of the references to color in this figure legend, the reader is referred to the web version of this article.)

cellular and structural information can be preserved at its original state and the morphodynamics can be analyzed in real time [20]. For the studies of bone tissues, the 1200–1300 nm excitation wavelength has the advantages of low scattering and absorption coefficients compared with visible and 800–1100 nm excitation [22]. Besides, THG modality provides label-free contrasts for the analysis of mineralization in bone development [23], cracks in human enamel [24], dentin tubules in fossil teeth [25], chondrocytes in mice ears [26], porosity and interfaces of bones [27], and osteocyte densities [28]. Most of these previous studies used *ex vivo* samples, and the information about cells may be lost. Here, we report and review the use of harmonic generation imaging of bone microenvironment *in vivo*. The star-shaped osteocytes and extended canaliculi can be easily observed in bone by THG contrast. In the bone marrow, we found THG contrast can highlight the granular leukocytes and the osteoblast on the wall of bone marrow cavities. Both bone repair process and hematopoietic stem cells niche can be studied based on this live imaging platform in the future.

2. Experimental setup

The laser source and imaging setup of this work have been mentioned in our previous report [6]. Basically, the laser source is a home-build femtosecond Cr:forsterite laser operating at 1250 nm. The pulse width is 100 fs, and the repetition rate is about 110 MHz. To initiate the mode-locking, the laser cavity uses a semiconductor saturable mirrors (SESAM). The SESAM consisted of 25 periods of GaAs/AlAs quarter-wave layers, followed by an $Al_{0.48}In_{0.52}As$ quarter wave layer with two embedded $Ga_{0.47}In_{0.53}As$ quantum wells. The laser beam was two-dimensionally scanned by a commercialized scanning unit (FV300, Olympus, Tokyo, Japan). A telescope lens tube was inserted between scanner and objective to form a $4f$ scanning structure. The scanning rays of the laser beam were converged to the back aperture of the objective, and the beam size was expanded to fit that of the back aperture. Before the objective, the laser beam transmitted through a multiphoton dichroic beam splitter with 865-nm edge wavelength. Finally, the laser beam was focused by a 60× water-immersion objective with a numerical aperture of 1.2 (UPLANSAPO, Olympus, Tokyo, Japan). The laser power after the objective was around 80 mW. The generated two-photon fluorescence (TPF), SHG, and THG signals were epi-collected by the same objective. The SHG and THG signals were reflected by the multiphoton dichroic beam splitter, separated by 490-nm edged dichroic beam splitters, and detected by photomultiplier tubes (PMT: R4220P for THG and R943-02 for SHG, Hamamatsu). The TPF signals of indocyanine green (ICG), an angiography dye, transmitted the multiphoton dichroic beam splitter, returned to the scanner and detected by the built-in PMT in the FV300 scanner (R928, Hamamatsu). The photocurrents from PMTs were converted to voltages and digitized by the analog to digital converter in the imaging system (Fluoview, Olympus). The assembled TPF, SHG, and THG images have 512 × 512 pixels at a 3 Hz frame rate.

3. Harmonic generation microscopy of mouse bone marrow in vivo

To image the bone microenvironment *in vivo*, we chose the calvarial bone marrow of an ICR mouse as the imaging site. The ICR mouse is a strain of albino mice originating in Switzerland and selected by Dr. Hauschka. The experimental procedure met the criteria outlined by the Institutional Animal Care and Use Committee of National Taiwan

Please cite this article in press as: P.-C. Wu, et al., Harmonic generation microscopy of bone microenvironment *in vivo*, Optics Communications (2018), https://doi.org/10.1016/j.optcom.2018.01.023.

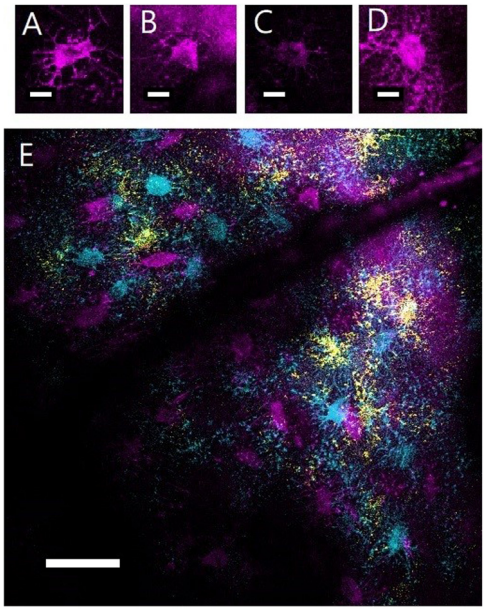

Fig. 2. (A–D) Third harmonic generation images of osteocytes within lacunae. Fields of view: 40 × 40 μm (E) Projected third harmonic generation images in Fig. 1 at different depths. Magenta, cyan, and yellow colors represent the image at the depth of 20 μm, 40 μm, and 60 μm, respectively. Fields of view: 240 × 240 μm. Scale bars: (A–D) 10 μm; (E) 40 μm. (For interpretation of the references to color in this figure legend, the reader is referred to the web version of this article.)

University (NTU-IACUC), and we handled the mice according to the guidelines in The Handbook of the Laboratory Animal Center, National Taiwan University. We performed all experiments as carefully as possible to minimize the suffering of the animals. The mouse was anesthetized with isoflurane. Its vital sign and body temperature were monitored and maintained (94–163 breaths/min, 325–780 beats/min, 37.5 °C). Then we used sterile forceps and scissors to open the skin and exposed the calvarium region for the imaging. For angiography, we tail-vein injected 100 μL of 0.5 mg/mL indocyanine green (ICG) as a contrast agent. The TPF signals of ICG at 870–1000 nm can be excited by the 1250 nm femtosecond pulses and detected by the PMT inside the scanner.

From the surface of the calvarial bone (d = 0 μm) down to an imaging depth of 60 μm, harmonic generation microscopy can reveal the distribution of lacuna/canaliculi (magenta color, Fig. 1) in bone (green color, Fig. 1). Each black hole in the SHG images is the lacunae of the osteocytes. Since the solid bone has a higher refractive index than the cells and interstitial fluids within lacunae cavities, the Gouy phase shift of focused Gaussian beam will give strong THG contrast at these interfaces of lacuna cavities and canaliculi. The difference in refractive indices further back-scattered the forward-generated THG signals and enhanced their THG contrasts. That is why lacuna has such strong THG contrast in bone. Inside each lacuna, at some sectioning planes, we could observe negative THG contrast [Fig. 2(A)–(D)]. Previously, we found the three-photon fluorescence contrast of interstitial fluids and the two-photon fluorescence contrast of labeled osteocytes did not overlap well in lacunae cavities [28], indicating that osteocytes did not occupy the whole lacunae cavities. A similar conclusion was drawn based on the transmission electron microscope images of bones [29]. Moreover, the osteocytes emanate many filopodia into the canaliculi spaces, holding osteocytes at the center of cavities [30]. According to these reports, this negative contrast of THG might be contributed by the major cell bodies of osteocytes, where material refractive indices are relatively homogeneous under the scale of excitation wavelength. Similar to the *ex vivo* results [27], the canaliculi fine structures can also be clearly resolved *in vivo* by the THG images (Figs. 1 and 2). Interestingly, our THG tomography also found nearby layers of osteocytes did not overlap vertically [Fig. 2(E)]. They transversely interleaved and formed a three-dimensional network connected by multiple canaliculi. When the imaging depth went down to 80 μm, we dived in a bone marrow cavity and observed the relative straight and thin arteriole (left, Fig. 3) [31] and winding sinusoid vessels (Fig. 3) revealed by the TPF imaging of tail-vein injected ICG. Since the sinusoidal vessels are fenestrated, the ICG-bounded albumin could leak out, and the densely packed bone marrow cells can be outlined (honey cone structures among vessels in Fig. 3). Some cells aggregated in the vicinity of sinusoids have strong THG contrast within (Fig. 3). According to our previous studies, red blood cells have strong THG contrast, and THG images can reflect the granularity of leukocytes [21]. These high-granularity cells might be the myelocytes, reticular cells, or plasma cells. The identity confirmation needs further studies with immunofluorescence labeling or transgenic labeled mice. Finally, on the wall of bone marrow cavity, we can find a lining of cells with strong THG signals (Fig. 4). Compared with anatomical images of bone marrow cavity [32], they could be either osteoblasts or osteoclasts.

4. Summary

In summary, we report the label-free harmonic generation microscopy of bone microenvironment *in vivo*. Although SHG and THG are not imaging modalities with molecular specificity, their morphological information allows the identification of osteocytes, lacunae, and connecting canaliculi inside the bone. Typically, SHG signals have a higher intensity than that of THG one. Their nuclei can be analyzed.

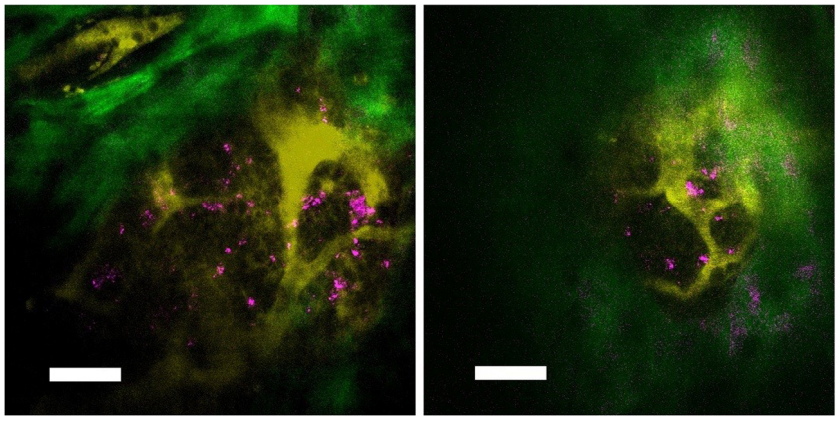

Fig. 3. Combined second harmonic generation (green color), third harmonic generation (magenta color), and two-photon fluorescence (yellow color) imaging of the calvarial bone marrow *in vivo*. Fields of view: 240 × 240 μm. Scale bars: 40 μm. (For interpretation of the references to color in this figure legend, the reader is referred to the web version of this article.)

Please cite this article in press as: P.-C. Wu, et al., Harmonic generation microscopy of bone microenvironment *in vivo*, Optics Communications (2018), https://doi.org/10.1016/j.optcom.2018.01.023.

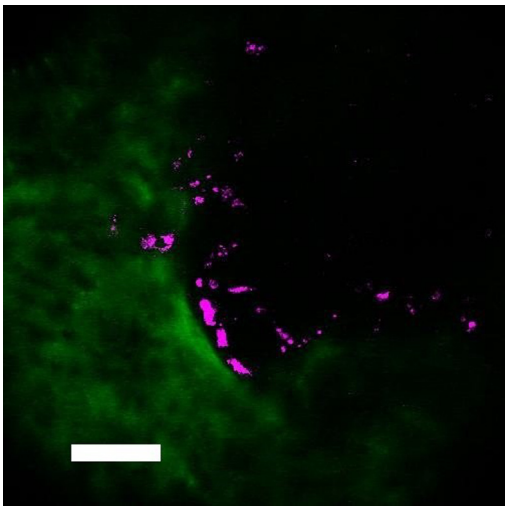

Fig. 4. Third harmonic generation imaging (magenta color) of cells lining on the wall (green color) of bone marrow cavity. Fields of view: 300 × 300 μm. Scale bar: 50 μm. (For interpretation of the references to color in this figure legend, the reader is referred to the web version of this article.)

Into the bone marrow cavity, combined with ICG angiography, THG images can see the granulocytes reside near the sinusoidal vessels and the osteoblast lining on the wall of bone marrow cavities. These findings provide a valuable background information for the future studies with fluorescence-labeled cells.

Acknowledgments

This work is sponsored by the Faculty of Health Sciences, University of Macau and supported by Science and Technology Development Fund (FDCT) of Macao SAR under grant number of 122/2016/A3.

References

[1] J. Squier, M. Müller, High resolution nonlinear microscopy: A review of sources and methods for achieving optimal imaging, Rev. Sci. Instrum. 72 (2001) 2855–2867.
[2] W. Denk, J.H. Strickler, W.W. Webb, Two-photon laser scanning fluorescence microscopy, Science 248 (1990) 73–76.
[3] S. Maiti, J.B. Shear, R.M. Williams, W.R. Zipfel, W.W. Webb, Measuring serotonin distribution in live cells with three-photon excitation, Science 24 (1997) 530–532.
[4] S.-W. Chu, I.-H. Chen, T.-M. Liu, C.-K. Sun, S.-P. Lee, B.-L. Lin, P.-C. Cheng, M.-X. Kuo, D.-J. Lin, H.-L. Liu, Nonlinear bio-photonic crystal effects revealed with multimodal nonlinear microscopy, J. Microsc. 208 (2002) 190–200.
[5] P.J. Campagnola, A.C. Millard, M. Terasaki, P.E. Hoppe, C.J. Malone, W.A. Mohler, Three-dimensional high-resolution second-harmonic generation imaging of endogenous structural proteins in biological tissues, Biophys. J. 82 (2002) 493–508.
[6] P.-C. Wu, T.-Y. Hsieh, Z.-U. Tsai, T.-M. Liu, In vivo quantification of the structural changes of collagens in a melanoma microenvironment with second and third harmonic generation microscopy, Sci. Rep. 5 (2015) 8879.
[7] S.G. Stanciu, S. Xu, Q. Peng, J. Yan, G.A. Stanciu, R.E. Welsch, P.T.C. So, G. Csucs, H. Yu, Experimenting liver fibrosis diagnostic by two photon excitation microscopy and bag-of-features image classification, Sci. Rep. 4 (2014) 4636.
[8] C.-M. Hsueh, W. Lo, W.-L. Chen, V.A. Hovhannisyan, G.-Y. Liu, S.-S. Wang, H.-Y. Tan, C.-Y. Dong, Structural characterization of edematous corneas by forward and backward second harmonic generation imaging, Biophys. J. 97 (2009) 1198–1205.
[9] J.D. Hutcheson, C. Goettsch, S. Bertazzo, N. Maldonado, J.L. Ruiz, W. Goh, K. Yabusaki, T. Faits, C. Bouten, G. Franck, T. Quillard, P. Libby, M. Aikawa, S. Weinbaum, E. Aikawa, Genesis and growth of extracellular-vesicle-derived microcalcification in atherosclerotic plaques, Nat. Mater. 15 (2016) 335–343.
[10] M.-R. Tsai, Y.-W. Chiu, M.T. Lo, C.-K. Sun, Second harmonic generation imaging of collagen fibers in myocardium for atrial fibrillation diagnosis, J. Biomed. Opt. 15 (2010) 026002.
[11] R. Kumar, K.M. Grønhaug, C.L. Davies, J.O. Drogset, M.B. Lilledahl, Nonlinear optical microscopy of early stage (ICRS Grade-I) osteoarthritic human cartilage, Biomed. Opt. Express 6 (2015) 1895–1903.
[12] J.M. Runnels, A.L. Carlson, C. Pitsillides, B. Thompson, J. Wu, J.A. Spencer, J.M. Kohler, A. Azab, A.S. Moreau, S.J. Roding, A.L. Fung, K.C. Anderson, I.M. Ghobrial, C.P. Lin, Optical techniques for tracking multiple myeloma engraftment, growth, and response to therapy, J. Biomed. Opt. 16 (2011) 011006.
[13] C.-K. Sun, S.-W. Chu, S.-Y. Chen, T.-H. Tsai, T.-M. Liu, C.-Y. Lin, H.-J. Tsai, Higher harmonic generation microscopy for developmental biology, J. Struct. Biol. 147 (2004) 19–30.
[14] N. Oliver, M.A. Luengo-Oroz, L. Duloquin, E. Faure, T. Savy, I. Veilleux, X. Solinas, D. Débarre, P. Bourgine, A. Santos, N. Peyriéras, E. Beaurepaire, Cell lineage reconstruction of early zebrafish embryos using label-free nonlinear microscopy, Science 329 (2010) 967–971.
[15] S.-Y. Chen, H.-Y. Wu, C.-K. Sun, In vivo harmonic generation biopsy of human skin, J. Biomed. Opt. 14 (2009) 060505.
[16] S.-Y. Chen, S.-U. Chen, H.-Y. Wu, W.-J. Lee, Y.-H. Liao, C.-K. Sun, In Vivo Virtual biopsy of human skin by using noninvasive higher harmonic generation microscopy, IEEE J. Sel. Top. Quantum Electron. 16 (2010) 478–492.
[17] M.-R. Tsai, S.-Y. Chen, D.-B. Shieh, P.-J. Lou, C.-K. Sun, In vivo optical virtual biopsy of human oral mucosa with harmonic generation microscopy, Biomed. Opt. Express 2 (2011) 2317–2328.
[18] L. Liu, J.A. Gardecki, S.K. Nadkarni, J.D. Toussaint, Y. Yagi, B.E. Bouma, G.J. Tearny, Imaging the subcellular structure of human coronary atherosclerosis using micro-optical coherence tomography, Nat. Med. 17 (2011) 1010–1014.
[19] L. Golan, D. Yeheskely-Hayon, L. Minai, E.J. Dann, D. Yelin, Noninvasive imaging of flowing blood cells using label-free spectrally encoded flow cytometry, Biomed. Opt. Express 3 (2012) 1455–1464.
[20] C.-K. Chen, T.-M. Liu, Imaging morphodynamics of human blood cells in vivo with video-rate third harmonic generation microscopy, Biomed. Opt. Express 3 (2012) 2860–2865.
[21] C.-H. Wu, T.-D. Wang, C.-H. Hsieh, S.-H. Huang, J.-W. Lin, S.-C. Hsu, H.-T. Wu, Y.-M. Wu, T.-M. Liu, Imaging cytometry of human leukocytes with third harmonic generation microscopy, Sci. Rep. 6 (2016) 37210.
[22] A.N. Bashkatov, E.A. Genina, V.I. Kochubey, V.V. Tuchin, Optical properties of human cranial bone in the spectral range from 800 to 2000 nm, in: Proc of SPIE. 2006; Vol. 6163, pp. 6163101–61631011.
[23] D. Oron, D. Yelin, E. Tal, S. Raz, R. Fachima, Y. Silberberg, Depth-resolved structural imaging by third-harmonic generation microscopy, J. Struct. Biol. 147 (2004) 3–11.
[24] S.-Y. Chen, C.-Y.S. Hsu, C.-K. Sun, Epi-third and second harmonic generation microscopic imaging of abnormal enamel, Opt. Express 16 (2008) 11670–11679.
[25] Y.-C. Chen, S.-Y. Lee, Y. Wu, D.-B. Shieh, K. Brink, T.D. Huang, R.R. Reisz, C.-K. Sun, Third harmonic generation microscopy reveals dental anatomy in ancient fossils, Opt. Lett. 40 (2015) 1354–1357.
[26] M.-R. Tsai, C.-H. Chen, C.-K. Sun, Third and second harmonic generation imaging of human articular cartilage, in: Proceeding of SPIE, Vol. 7183, 2009, pp. 71831V-1–71831V-10.
[27] R. Genthial, E. Beaurepaire, M.-C. Schanne-Klein, F. Peyrin, D. Farlay, C. Olivier, Y. Bala, G. Boivin, J.-C. Vial, D. Débarre, A. Gourrier, Label-free imaging of bone multiscale porosity and interfaces using third-harmonic generation microscopy, Sci. Rep. 7 (2017) 3419.
[28] D. Tokarz, R. Cisek, M.N. Wein, R. Turcotte, C. Haase1, S.-C.A. Yeh, S. Bharadwaj, A.P. Raphael, H. Paudel, C. Alt, T.-M. Liu, H.M. Kronenberg, C.P. Lin, Intravital imaging of osteocytes in mouse calvaria using third harmonic generation microscopy, PLoS One 12 (2017) e0186846.
[29] X. Lai, C. Price, S. Modla, W.R. Thompson, J. Caplan, C.B. Kirn-Safran, L. Wang, The dependences of osteocyte network on bone compartment, age, and disease, Bone Res. 3 (2015) 15009.
[30] S.A. Kamel-ElSayed, L.M. Tiede-Lewis, Y. Lu, P.A. Veno, S.L. Dallas, Novel approaches for two and three dimensional multiplexed imaging of osteocytes, Bone 76 (2015) 129–140.
[31] T. Itkin, S. Gur-Cohen, J. Spencer, A. Schajnovitz, S. Ramasamy, A. Kusumbe, G. Ledergor, Y. Jung, I. Milo, M. Poulos, A. Kalinkovich, A. Ludin, K. Golan, E. Khatib, A. Kumari, O. Kollet, G. Shakhar, J. Butler, S. Rafii, R. Adams, D. Scadden, C. Lin, T. Lapidot, Distinct bone marrow blood vessels differentially regulate haematopoiesis, Nature 532 (2016) 323–328.
[32] J.S. Khurana, F.F. Safadi, Bone Structure, Development and Bone Biology, in: Essentials in Bone and Soft-Tissue Pathology, Springer, Boston, MA, 2010.

Please cite this article in press as: P.-C. Wu, et al., Harmonic generation microscopy of bone microenvironment *in vivo*, Optics Communications (2018), https://doi.org/10.1016/j.optcom.2018.01.023.